PROGRESS IN PHOTOVOLTAICS: RESEARCH AND APPLICATIONS
Prog. Photovolt: Res. Appl. (2011)
Published online in Wiley Online Library (wileyonlinelibrary.com). DOI: 10.1002/pip.1110

RESEARCH ARTICLE

17.9% Metal-wrap-through mc-Si cells resulting in module efficiency of 17.0%

M. W. P. E. Lamers[1]*, C. Tjengdrawira[1], M. Koppes[1], I. J. Bennett[1], E. E. Bende[1], T. P. Visser[1], E. Kossen[1], B. Brockholz[1], A. A. Mewe[1], I. G. Romijn[1], E. Sauar[2], L. Carnel[3], S. Julsrud[3], T. Naas[3], P. C. de Jong[1] and A. W. Weeber[1]

[1] ECN Solar Energy, P.O. Box 1, 1755 ZG Petten, The Netherlands
[2] REC Group, P.O. Box 594, 1302 Sandvika, Norway
[3] REC Wafer, Tormod Gjestlandsvei 41, 3908 Porsgrunn, Norway

ABSTRACT

We obtained 17.9% cell efficiency on thin and large mc-Si REC wafers using ECN's metal-wrap-through (MWT) concept. Optimization of several cell processing steps led to an increase of more than 2% absolute in cell efficiency. With these cells 36-cell modules were manufactured at 100% yield in our industry scale module pilot line. The highest module efficiency obtained (as independently confirmed by JRC-ESTI) was 17%. In this module the average cell efficiency was 17.8%; this shows a small difference between cell and module efficiency. Copyright © 2011 John Wiley & Sons, Ltd.

KEYWORDS

multi crystalline silicon; metal-wrap-through; module integration; high-efficiency module; high-efficiency cells; world record

***Correspondence**

M. W. P. E. Lamers, ECN Solar Energy, P.O. Box 1, 1755 ZG Petten, the Netherlands.
E-mail: lamers@ecn.nl

Received 14 September 2010; Revised 15 December 2010

1. INTRODUCTION

To reach grid parity, PV industry focuses on obtaining higher efficiencies, while simultaneously reducing material and process costs. In this article we will show that this goal can be obtained with ECN's integrated metal-wrap-through (MWT) cell and module concept. Both can be manufactured with a very high yield, which is another requirement to be industrially viable. To underline our motivation for developing the ECN-MWT cell and module concept, first conventional H-pattern processing and bottlenecks are explained.

Conventional solar cells are based on so-called H-pattern front-side metallization: two large busbars with connecting fingers on the front side and two large busbars or pads on the full aluminum rear side. In module fabrication the front and rear side of in series placed solar cells are interconnected with tabbing strips or ribbons.

Several problems that reduce yield and efficiency can occur in H-pattern cell and module fabrication; some are illustrated in Figure 1.

Higher efficiencies and related higher currents increase the series resistance in the module's interconnection material. A higher series resistance is also caused by an increase in the finger length when larger cells are used (1). Reducing the finger length by using three busbars will increase the shading losses due to higher metallization coverage (2). Cell bowing due to the full aluminum rear-side metallization can lead to increased breakages during module manufacturing process, in particular for thinner cells (3). Additional cell breakages can be expected at the edges of thin cells by the tabbing material used in conventional module manufacturing (4). Also, the soldering of the strips creates a highly stressed surface that may lead to increased breakages during module manufacturing (5).

These drawbacks are overcome by the ECN-MWT cell and module concept [1]. In Figure 2 a photo of an ECN-MWT cell is shown. In one cell, 16 unit cell structures (4×4) are used. In the middle of the unit cell structure a laser hole is drilled through which the emitter metal contacts are wrapped, realizing all electrical contacts on the rear. An illustration of the cross-section of the ECN-

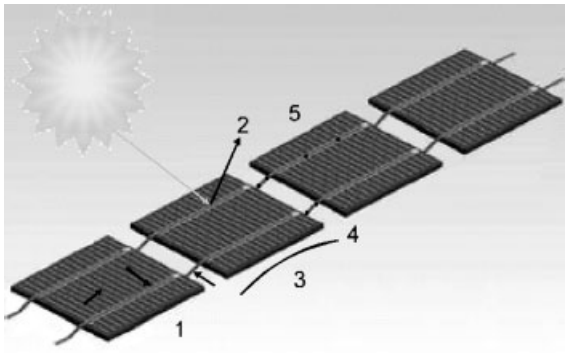

Figure 1. Problems in H-pattern module fabrication: series resistance in fingers and interconnection material (1), increase of shading losses if more busbars are used (2), cell bowing (3), cell breakage at edges (4), and at soldering points (5).

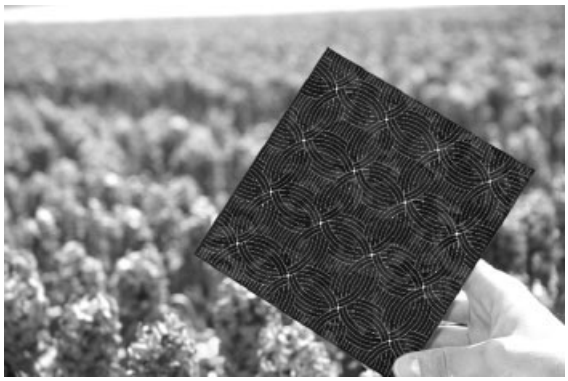

Figure 2. Photograph of a 243 cm^2 back-contacted MWT cell.

MWT cell can be seen in Figure 3. The design of the metal patterning of the ECN-MWT solar cell is significantly different as compared to MWT designs by other groups [2–4]. As already described above, the ECN-MWT cell uses unit cell structures while others use pattern design based on straight lines. In the ECN-MWT design only 16 holes are required, while others need much more holes (in the order of 100) for their design is based on lines. An additional advantage of the ECN-MWT design is that it allows a very easy up-scaling of the wafer size by a simple addition of more unit cell structures without increases in series resistance or shading losses. In previous work by ECN and by others [2–4] it was demonstrated that a significant gain in efficiency can be obtained using a MWT concept as compared to the conventional H-pattern processing. For the ECN-MWT cell and other MWT cell designs, the metallization front-side coverage of about 5.5% resulted in a 2–3% relative gain in J_{SC} as compared to an H-pattern cell with had a metallization coverage of 7.5% [1–6].

For the ECN-MWT module manufacturing a low-series resistance is obtained by contacting the cells to a conductive foil using a conductive adhesive (CA). For H-pattern cells, it was already demonstrated using damp-heat and thermal-stress tests that the application of CAs between busbars and tabs provides low-stress interconnection and a highly stable contact [7]. ECN's MWT conductive foil for interconnection is covered with an isolation layer with local openings. On these locations the CA is printed which connects the cell to the foil. This way of module fabrication of ECN-MWT solar cells results in a high yield, especially even for thin cells. As the cells are glued on the foil using a CA no soldering stress or stress at the edges of the cells is present. Additionally, this method of module fabrication allows a higher packing density as no tabs are needed in between the cells. Also, the required area for bussing can be omitted, as this is integrated in the function of the interconnection foil and thus no additional area is needed. The use of the conducting foil allows more efficient current collection over the whole cell area as compared to conventional 2 mm tabs. Finally, module manufacturing can be done 3–8 times as fast (depending on module size) as conventional module fabrication up to the lamination process. It has been demonstrated that a 2% relative gain in FF and a 1% relative gain in J_{SC} can be obtained at the module level [1,8].

The module integration of these cells, where the advantage of the ECN-MWT cell concept is most evident, resulted in world record module efficiency for mc-silicon of 17.0% [9]. At the time of writing, the world record module efficiency has been further increased by Kyocera using another MWT technology (17.3%) [10] and Schott Solar using H-pattern PERC design (17.6%) [11].

Cost calculations for the ECN-MWT module show PV module direct manufacturing costs of about 1 €/Wp, which is needed to enable grid parity [12]. Also, the IEC certificate 61215 was obtained for this method of module manufacturing [13].

2. ECN-MWT CELL AND MODULE PROCESSING

Industrial ECN-MWT cell processing, which is based on screen-printing, closely resembles conventional industrial

Figure 3. Illustration of a cross-section of the MWT cell. More details can be found in Refs. [1,5,6].

Table I. Industrial H-pattern and ECN-MWT solar cell processing on 243 cm^2 mc-Si wafers.

Process sequence mc-Si cells
Laser drilling of holes
Texture
Emitter formation
Glass removal and cleaning
Front-side SiN_x:H deposition
Screen-printing of the Ag front side, **Ag holes**, Ag rear side, and Al rear-side metallization
Simultaneous firing
Laser isolation around the **holes** and edge

The additional steps required to fabricate an ECN-MWT cell are printed bold.

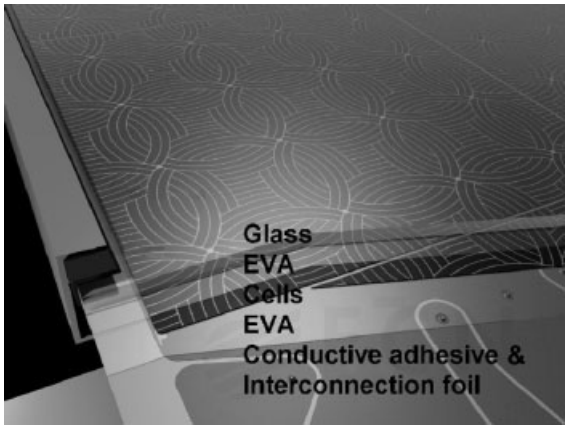

Figure 4. Illustrative image of the MWT module, showing the placement of the different components.

H-pattern processing; the main differences are the laser drilling, metallization, and isolation of the holes. The cell process flow is given in Table I.

Cell manufacturing of the ECN-MWT cell starts with laser drilling of the holes. Removal of saw and laser damage is combined with a wet-chemical texturing step. Subsequently, emitter formation is carried out by high-temperature phosphorus diffusion. After glass removal and cleaning, a SiN_x:H anti-reflection and passivation coating is applied on the front side of the wafer. Metallization of the front side, the holes and the rear side is done by screen-printing. The contacts are formed by a short high-temperature step (peak firing). The final step is laser isolation of the edge and around the holes.

The module process flow is giving in Table II. Module manufacturing using our automated pilot line has been reported before [14]. An illustrative image of a cell in the module, which shows the placement of the different components, is given in Figure 4.

Up to the lamination step, ECN-MWT module building is 3–8 times faster as compared to conventional H-pattern module build, using tabber-stringer. Process steps 1–6 can each be performed within 1 min for a 60-cell module.

The module build begins with the placement of a patterned conductive foil to a carrier plate using vacuum. The CA, which realizes the electrical contact between the foil and metallization of the cell, is printed on the foil. The rear-side encapsulant is perforated at the positions where the CA is printed to allow contact with the cells and is placed on the foil. Subsequently, the cells are individually picked from a stack by a robot and placed on the foil such that the contacts on the cell make contact with the CA. As a last step before lamination the sheet of encapsulant and glass is placed on the front side of the cells. During lamination the cells are encapsulated by the encapsulant and the CA is cured simultaneously, which secures the electric contact between the cells and the foil. This is shown in Figure 5. The module is finalized by the placement of the junction box and frame.

Table II. Industrial ECN-MWT solar module processing.

Process sequence ECN-MWT module
Placement interconnection foil
Screen printing conductive adhesive
Puncturing rear-side sheet of encapsulant and placement on foil
Pick and place of ECN-MWT cells
Placement of front-side sheet of encapsulant
Placement of glass
Lamination
Finishing module assembly (placement junction box and frame)

3. EVOLUTION OF ECN-MWT CELLS

To show the progress made with ECN-MWT the efficiency distribution on mc-Si cells from the last 6 years is depicted in Figure 6. It can be seen that since the first cells processed in 2003 efficiencies rapidly increased due to various improvements, which led to the definition of a ECN-MWT industrial process flow in 2006. The process steps for this flow are given in Table I. Further optimizations in the process flow in 2008 and 2009 led to a top cell efficiency of 17.9%, an average cell efficiency of 17.8% on 36 cells, and when integrated in module to a module efficiency on aperture area of 17.0%. During the same time period wafer size increased from 225 to 243 cm^2 and cell thickness decreased from 240 to 160 μm. In the next section the optimizations made relative to the process flow as defined in 2006 are discussed.

4. ECN-MWT CELL PROCESS OPTIMIZATION 2006–2009

The ECN-MWT processing has been optimized on several aspects and these are described in this section. In all cases

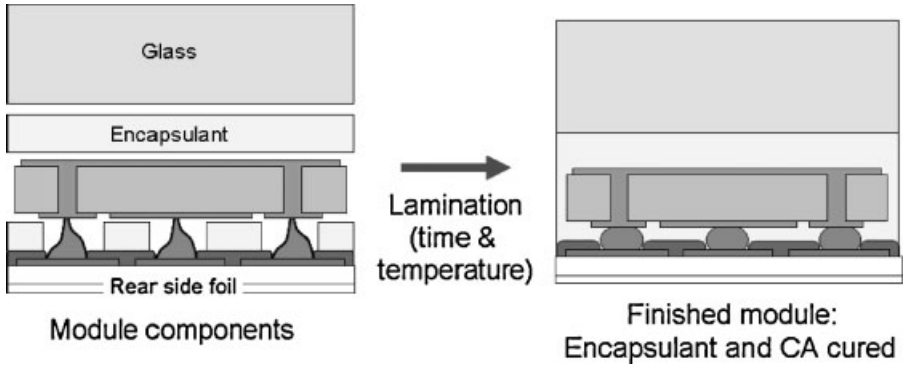

Figure 5. During lamination both the encapsulant and CA are cured.

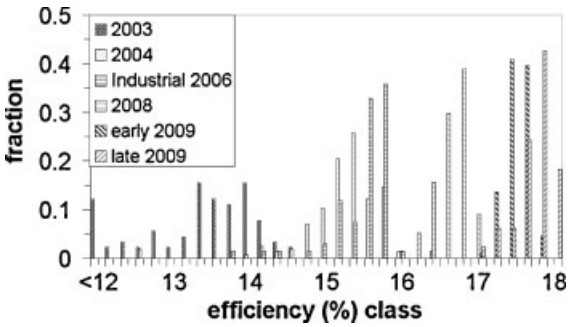

Figure 6. ECN-MWT efficiency throughout the years. When required, efficiencies are recalculated to the new spectrum as defined by Green [16]

1–1.5 Ω · cm 160 μm thin mc-Si p-type cells, sized $156 \times 156\,mm^2$, were used, unless stated otherwise. The current–voltage (*IV*) measurements on cells were performed according to the ASTM-E948 standard [15] using the class A solar simulator at ECN and were measured or recalculated to the new spectrum as defined by Green *et al.* [16]. Implied V_{OC} and J_{0e} were determined using a Sinton Consulting WCT-120 lifetime tester [17,18]. SiN_x:H bond densities were determined using Fourier transform infrared (FTIR) spectroscopy. The bond densities were calculated by integrating the different absorption peaks over the frequency. Reflectance was measured using an integrating sphere.

4.1. Laser drilling of the holes

In the as-cut wafers 16 holes were drilled with a 355 nm UV laser. The width variation in the hole was less than 10% and the width variation from hole to hole was less than 2%. The width of the hole is smaller than 500 μm.

4.2. Texturing

In previous work it was shown that the use of an improved acidic etch T2 for saw damage removal and surface texturing results in a low reflection (Figures 7 and 8) [19]. This texture gave a relative increase of 3% in J_{SC} as compared to conventional acidic etch T1 on H-pattern cells. The use of the improved texture gives a similar result when applied on ECN-MWT cells.

4.3. Emitter

The emitter determines the diode characteristics of the cell. V_{OC}, J_{SC}, and FF are to a large account dependent on the emitter quality. To improve the diode characteristics the emitter recombination current J_{0e} needs to be reduced; this will improve V_{OC} and J_{SC}. In Figure 9 the relationship between J_{SC}/J_{0e} and $V_{OC,}$ using the ideal diode law relation $V_{OC} \approx \ln\left(\frac{J_{SC}}{J_{0e}}\right)$, is shown for different emitters as measured on textured neighboring p-type mc-Si wafers, respectively, cells. It is noted that the determination of J_{0e} on neighboring mc-Si wafers as has been done here only serves to obtain a relative comparison and does not give an absolute value of J_{0e}, as this also includes material

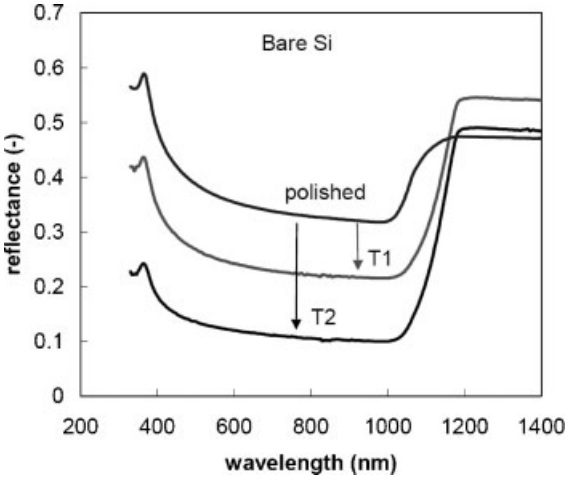

Figure 7. Reflectance of improved texture T2 as textured.

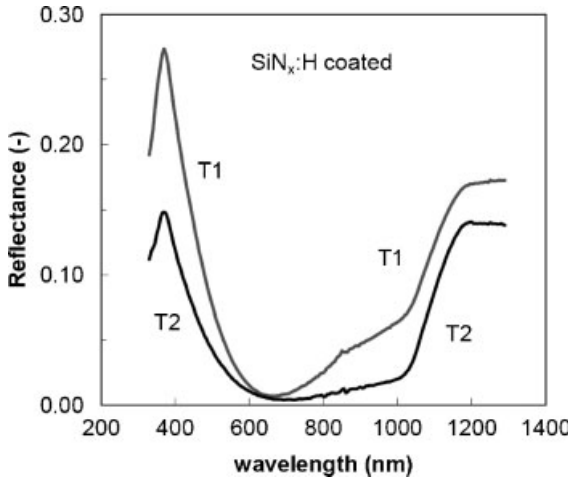

Figure 8. Reflectance of improved texture T2 when coated with SiN_x:H.

properties. It is also noted that the ideal diode law is not directly applicable to real solar cells. We use only the general relation between V_{OC}, J_{SC}, and J_{0e} described in the ideal diode law.

A high recombination is related to a high concentration of phosphorus in the emitter. Increasingly higher doping levels result in increasingly higher Auger recombination [20]. Additionally, precipitates can form, band gap narrowing occurs and crystal defects are formed at high-diffusion temperatures [21]. Reduction of the doping level will thus result in a lower recombination and therefore higher V_{OC} and J_{SC}. However, a high-phosphorus doping concentration is required to secure a good contact with the metallization and to obtain a high FF. The relationship between the phosphorus surface concentration and the FF that was found for our emitters is depicted in Figure 10.

Relatively simple optimization of the emitter can be done by reducing the depth of the highly doped region. In Figure 11, SIMS-plots are shown of two emitters, both having a high P-surface concentration. The in-line emitter has a J_{0e} of 450 fA/cm^2 as measured on textured mc-Si. The second one is a $POCL_3$ tube furnace emitter with a J_{0e} of

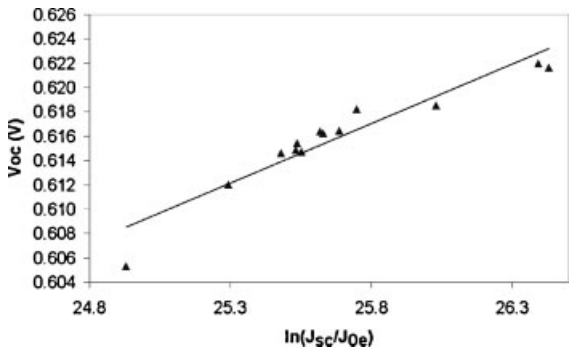

Figure 9. The relationship between J_{SC}/J_{0e} and V_{OC}.

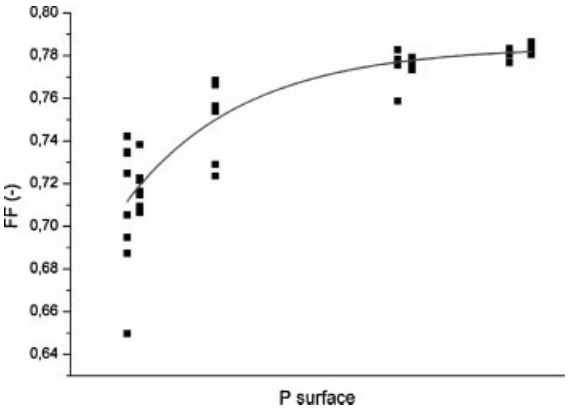

Figure 10. The relationship between doping concentration of phosphorus on the surface and the FF.

275 fA/cm^2. This lower J_{0e} is due to a significant decrease in dopant concentration at depths 30–70 nm from the surface. This gave an increase of 0.5% absolute in cell efficiency, while the FF remained at 78%. The cell results are presented in Table III.

4.4. SiN_x:H

SiN_x:H layers are commonly used as an anti-reflection coating. Additionally, the SiN_x:H provides bulk passivation by diffusion of hydrogen from the layer in the silicon and gives excellent surface passivation on n-type doped emitters due to both field and defect passivation. The composition of SiN_x:H can be optimized to obtain both good light coupling and optimal passivating qualities. The light coupling parameters (refractive index, thickness, and low absorption) can be optimized to the texture, the IQE of the cell and the glass, and encapsulant used in the module fabrication. The amount of bulk passivation required depends on the wafer quality, while the required surface passivation depends on the texture and emitter.

The SiN_x:H layers were deposited using in-line Micro Wave Remote PECVD system.

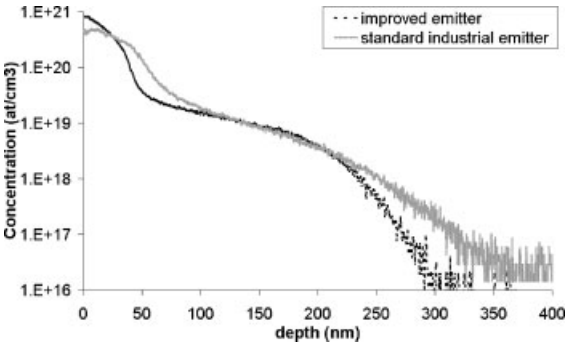

Figure 11. SIMS profiles of two emitters: a conventional industrial emitter and an improved emitter.

Table III. Cell parameters of neighboring H-pattern cells using two different emitters.

Average of nine cells	J_{SC} (mA/cm^2)	V_{OC} (mV)	FF	Efficiency (%)
Improved emitter	34.5	615	0.780	16.6
Conventional emitter	34.0	605	0.781	16.1

Low-quality mc-Si material needs very good bulk passivation to achieve maximum cell results; the bulk passivation property of the layer can be related to the Si−N bond density, the optimum value was found by Romijn *et al.* [22] to be between 1.2×10^{23} and 1.3×10^{23} cm^{-3} as shown in Figure 12. Lower Si−N bond densities correlate with a lower density and higher hydrogen content, whereas, higher Si−N bond densities correlate with a higher density and lower hydrogen content [23,24]. A SiN_x:H with higher hydrogen content gives a very good surface passivation, but a more dense structure is required to avoid too much out diffusion of H to the environment instead of to the Si bulk. Very good material quality (FZ material) does not desire any bulk passivation and the (implied) V_{OC} depends primarily on the surface passivation. This requires lower Si−N bond densities below 1.15×10^{23} cm^{-3}. In good quality mc-Si material a balance between bulk and surface passivation is called for and that this is the case can be seen in Figure 12. An optimum over a broad range for the Si−N bond density can be seen from 1.05×10^{23} to 1.35×10^{23} cm^{-3}.

By fine tuning the Si−N bond density as well as the light coupling parameters to the wafer quality, texture, emitter, IQE of the cell, and the module components specific for high-efficiency ECN-MWT cells, a gain in efficiency was achieved of at least 0.1% absolute compared to a broader range optimized SiN_x:H.

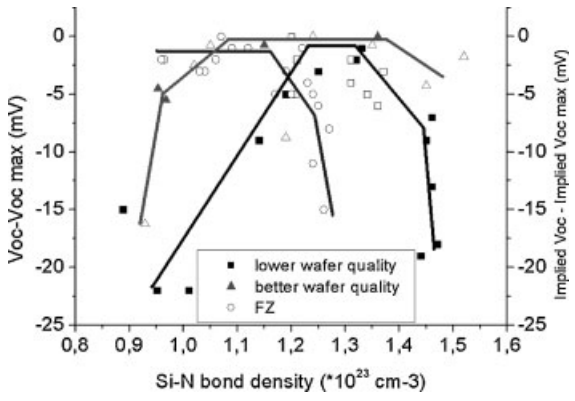

Figure 12. V_{OC}–V_{OC} (max) of mc-Si solar cells versus the Si−N bond density for lower and better mc-Si wafer quality and implied V_{OC}–V_{OC} (max) for half-fabricated FZ p-type wafers. Closed symbols: nitrides using N_2 as precursor gas; open symbols: nitrides using NH_3 as precursor gas. The lines are guides to the eye.

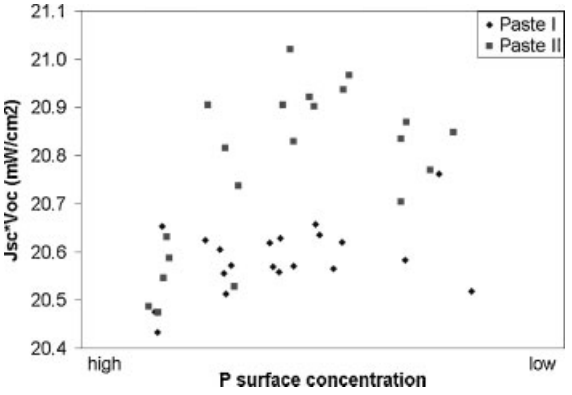

Figure 13. $J_{SC} \times V_{OC}$ as function of the P-surface concentration using two different front-side pastes on neighboring mc-Si cells.

4.5. Emitter contacting

Emitter optimization is closely related to a good emitter contact. V_{OC} and FF can be reduced due to increased recombination at the metal–Si interface. Different screen print pastes show different behavior. In Figures 13 and 14 this influence can clearly be seen in a comparison between two pastes on emitters with varying phosphorus surface concentration. Paste II shows a significantly higher $J_{SC} \times V_{OC}$, indicating that the recombination is lower at the interface between paste and emitter, while for Paste II this recombination is a clear dominant factor reducing the efficiency. In the experiment, the two pastes gave similar FF and also the line conductivity, width, and height were comparable [25]. A reduction in $J_{SC} \times V_{OC}$ was observed when the phosphorus doping level of the emitter became too low. This can be related to a too bad contact and lower FF [26].

4.6. Metal-wrap-through

The most significant difference between a ECN-MWT and an H-pattern cell is the metallization through the hole. By

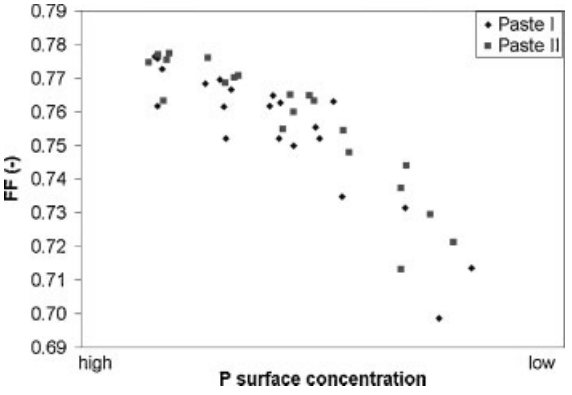

Figure 14. FF as a function of the P-surface concentration using two different front-side pastes on neighboring mc-Si cells.

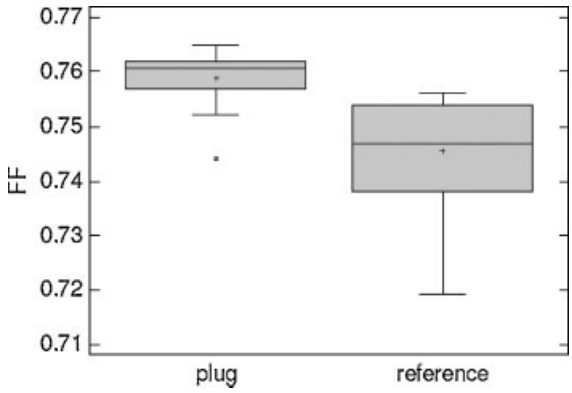

Figure 15. A significant improvement in FF is found when the holes are filled with an innovative plug paste as shown in this Box–Whisker plot.

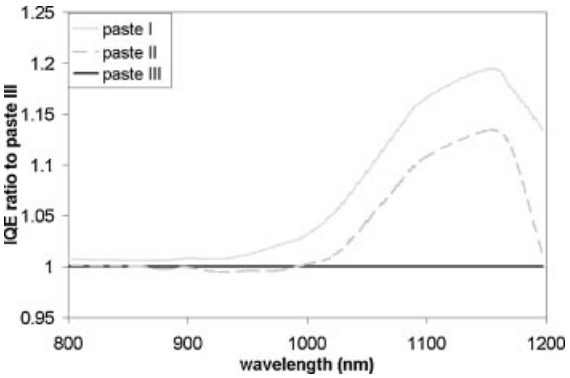

Figure 17. IQE ratio relative to paste III.

improving the conductivity through the holes by optimizing the metallization, the FF was significantly enhanced as shown in previous work [27]. The metallization was improved by using the innovative plug paste which fills the hole with Ag. The increase in FF relative to the original ECN-MWT metallization as defined in 2006 (reference) is indicated in the Box–Whisker plot shown in Figure 15. The improved distribution of the FF is mostly related to significantly better process stability. The use of the plug paste is not limiting the FF as values up to 0.787 have been obtained with our ECN-MWT concept.

4.7. Rear-side aluminum

The Al metallization on the rear side has the triple function of being the rear conductor, rear reflector, and rear-side passivation layer through the back-surface-field (BSF) formation. Also, a good contact with the Ag rear pads needs to be realized, as these will be the connection points to the module foil. In Figures 16 and 17 the results of a comparison study between different Al pastes are shown.

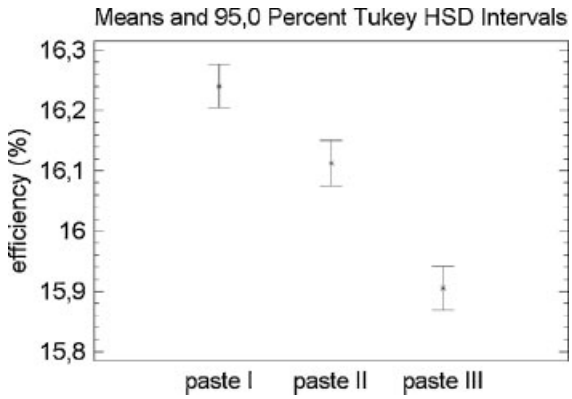

Figure 16. Efficiency of the different pastes.

The use of pastes I and II resulted in an efficiency gain of 0.3 and 0.2% absolute as compared to paste III. The gain was found in both J_{SC} and V_{OC}. In the EQE, IQE, and reflection data an increase in the red response (starting at ~900 nm) was observed. The improvements in rear-side reflection for pastes I and II accounted for, respectively, relatively 0.5 and 0.3% increase in J_{SC} relative to paste III. The remainder of the efficiency increase is due to improvements in the BSF passivating quality as indicated by the IQE, shown in Figure 17. These improvements can be related to the quality of the pastes, for example, the Al particle size. The Al particle size was significantly larger for paste II compared to paste I (unknown for paste III), while the Al percentage within the pastes was comparable and the amount of paste applied similar. Pastes containing smaller Al particles have been shown to give a more homogeneous BSF and, therefore, higher J_{SC} [28].

4.8. Isolation

Isolation of the diode by laser scribing is a conventional method in industry. Also chemical isolation is sometimes used as it typically leads to higher cell efficiencies. For the ECN-MWT cell, the edges and the holes need to be isolated. This means that not only the total length of laser grooves and the associated recombination is increased, but also that these recombination areas are positioned throughout the cell's surface and not only at the edges. Reduction of the laser damage is thus important to improve cell output, as shown in Figure 18. For the ECN-MWT cells, the standard laser processing was optimized and compared to chemical isolation. Optimizing the standard laser process led to an enhanced FF. This can be explained by reduced laser damage as the optimized laser grooves are narrower (from 100 to 30 μm) and shallower (from 20 to 6 μm). Microscopic images of the two laser grooves are shown in Figure 19. The chemical isolation gave an even better performance and led to the best fill and pseudo-fill factor.

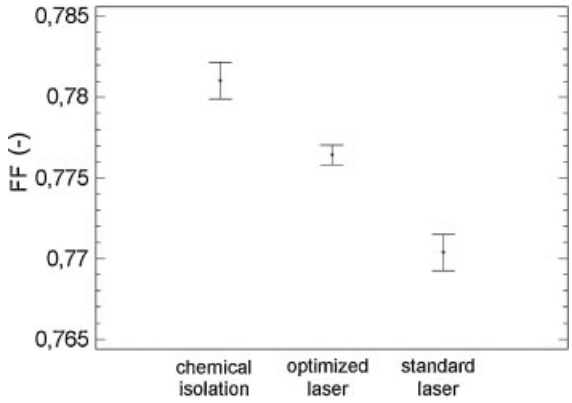

Figure 18. Different isolation methods and their effect on the FF.

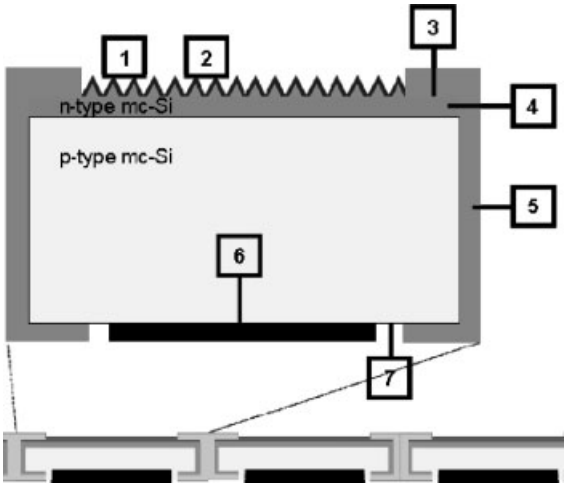

Figure 20. Locations of different optimizations in the ECN-MWT concept. Explanation of numbers is given in Table IV.

4.9. Front-side metallization pattern

The front-side metallization pattern can be optimized when the following parameters are known: base resistance, emitter resistance, emitter contact resistance, line resistivity, line width, and expected J_{SC} and V_{OC} (based on material quality and the used cell processes). Using these as input parameters and optimal pattern for the ECN-MWT cells was calculated, which gave a relative reduction in the front-side metallization area of close to 20% compared to the pattern as defined in 2006. This allowed an increase in $J_{SC} \times V_{OC}$ of 0.3% absolute.

4.10. Integration of optimized steps

Integration of all the optimized process steps, indicated by steps 1–7 in Figure 20 and Table IV, should lead to an increase of close to 1.8% absolute as compared to the ECN-MWT process flow as defined in 2006. The average ECN-MWT cell efficiency in 2006 was 15.5%, therefore, average cell efficiencies of 17.3% were to be expected.

Integration of the found optimizations led to an average cell efficiency of 17.6% over 81 cells. This is an improvement of 2.1% absolute since 2006. The best cell had an efficiency of 17.9%. The cell efficiencies are shown in Figure 21. The wafer material was p-type mc-Si provided by REC, sized $156 \times 156\,mm^2$ with a base resistivity of 1–1.5 $\Omega \cdot$ cm; the cell thickness was 160 μm. The wafer material was optimized by lowering the dislocation density. Two main reasons can be given for the discrepancy between the calculated 1.8% and the obtained 2.1%. These are the improved material quality and the positively mutual reinforcement of the multiple improvements.

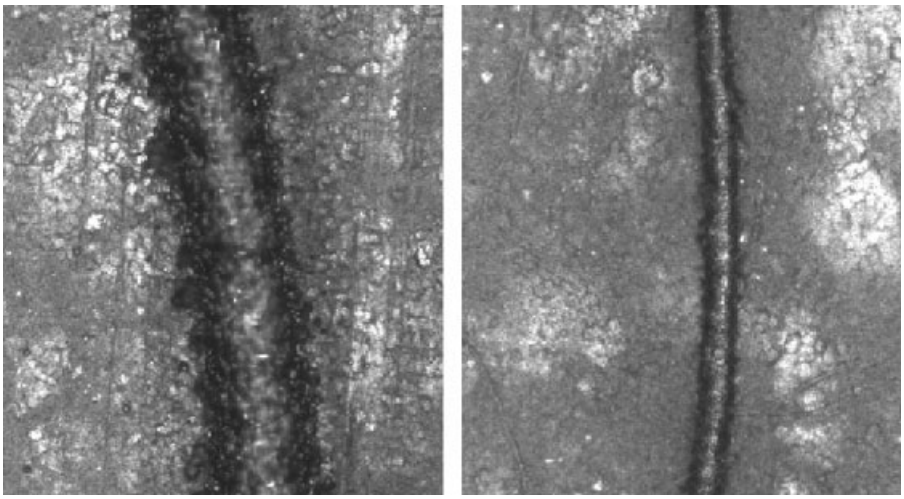

Figure 19. Left: Laser groove of standard laser. The groove is 100 μm wide and 20 μm deep. Right: Laser groove of optimized laser. The groove is 30 μm wide and 6 μm deep.

Table IV. When separate gains in efficiency are added, an absolute increase in efficiency of 1.8% can be expected relative to the industrial process flow as defined in 2006.

No.	Process step	Absolute gain in efficiency (%)
1	Improve texture and lower reflection	0.3
2	Improve SiN_x:H anti-reflection coating	0.1
3a	Improve emitter contact	0.15
3b	Improve front-side metallization pattern	0.3
4	Improve emitter	0.5
5	Improve conductivity in holes	0.15
6	Improve p-type contact	0.1
7	Improve isolation	0.2
	Total	1.8

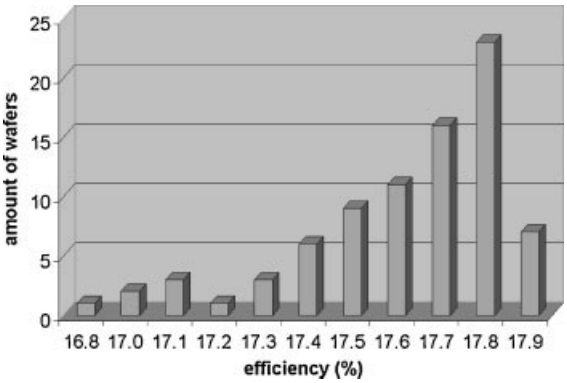

Figure 21. Cell efficiencies of MWT cells on REC material.

5. 17% MODULE EFFICIENCY

From the 81 processed cells, 36 cells were selected and integrated in a 9×4 ECN-MWT module. The module efficiency of 17% was independently confirmed by JRC-ESTI. Cell and module efficiencies are given in Table V. The module aperture area was 0.8885 m^2. Multiple ECN-MWT modules were manufactured at ECN with 100% yield, also when thinner cells of 120 μm were used [29]. A photo of a 60-cells mc-Si ECN-MWT module is shown in Figure 22.

The light coupling parameters of the cell are optimized for use under glass, allowing a higher J_{SC} in the module. Additionally, a special coating provided by Royal DSM N.V. was applied on the glass improving the light coupling even further, this increased J_{SC} with 1.6% absolute. As the packing ratio is not 100% in the module a very small loss of 1.4% in J_{SC} was found due to the packing ratio of close to 99%. Consequently, the J_{SC} of the cells before encapsulation is comparable to the J_{SC} of the finished module. A small loss of only 3% in FF was found due to the low resistance losses in the module components. The spectral response (SR) of an ECN-MWT cell and the module are given in Figure 23. It can be seen that the SRs are very similar, as is expected from the processing and the similar J_{SC}. At wavelengths shorter than 400 nm there are additional losses in the module. This loss can be explained by the absorption in the EVA (see below as well).

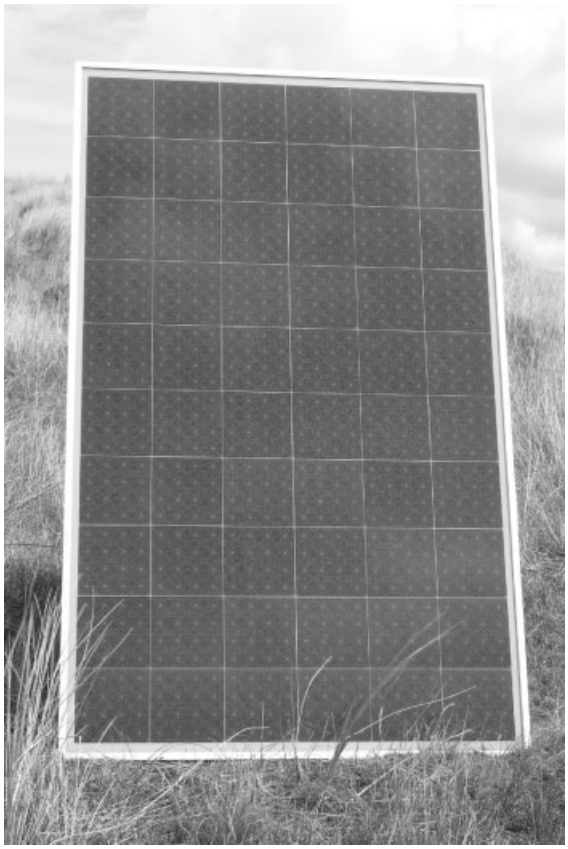

Figure 22. Photograph of a 60-cells mc-Si ECN-MWT module.

Main losses in the ECN-MWT cell, compared to an idealized but simple SR, are related to recombination at the

Table V. Cell and module efficiencies.

	Area (cm^2)	J_{SC} (mA/cm^2)	V_{OC} (V)	FF	Efficiency (%)
Best cell	243.36	36.41	0.632	0.778	17.9
Average 36 cells before encapsulation	243.36	36.37	0.631	0.774	17.8
Average 36 cells after encapsulation	243.36	36.94	0.630	0.750	17.2
Module (aperture area)	8885	36.41	22.67	0.750	17.0

Cell efficiencies are measured with a class A solar simulator at ECN and module efficiency is independently measured by JRC-ESTI.

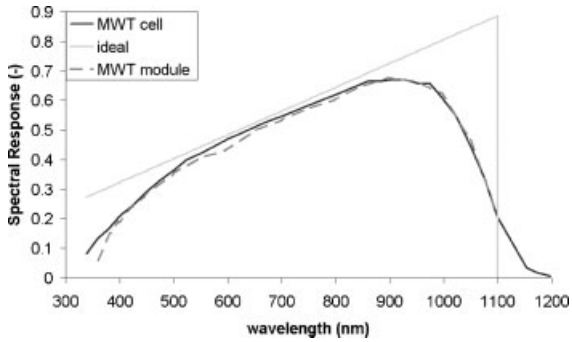

Figure 23. SR of a MWT cell and the MWT module. Also given is the idealized and simplified SR (QE = 1).

surfaces, in the emitter and in the bulk of the cell, and to the non-optimal light confinement. Recombination at the front surface and in the emitter, and absorption in the SiN_x:H reduce the response below 550 nm. The non-optimal bulk of the cell and rear-side properties (reflection and passivation) reduce the response for wavelengths above 900 nm.

6. LOSSES AND GAINS

Characterization of the high-efficiency ECN-MWT cells and the 17.0% module indicated three main topics in which a significant gain in efficiency can be obtained for the used material:

(1) Transmission of light to improve J_{SC}.
(2) Emitter recombination to improve J_{SC} and V_{OC}.
(3) Rear-side passivation and reflection to improve J_{SC} and V_{OC}.

6.1. Transmission of light

The transmission of light is reduced by several factors: on the module side by the reflection and absorption of the module glass and EVA, on the cell side by the reflection and absorption of the SiN_x, and by the reflection at the cell surface.

Reflection losses on the module side can be reduced with an anti-reflection coating on the glass. The 17% module had a special anti-reflection coating from Royal DSM N.V. which gave a gain of 1.6% relative in J_{SC}. Absorption in the module is mostly related to EVA, which is used in conventional module manufacturing. EVA absorbs all light of wavelengths below 400 nm, which accounts a 1–2% relative loss in J_{SC} [30]. Replacing EVA with another encapsulant which absorbs significantly less, like silicone, can give a gain of 0.7–1.1% relative in J_{SC} depending on the quality of the glass and the response of the cell at short wavelength [31].

To reduce the reflection losses on the cell side an improved texture was used which increased J_{SC} with 3% relative as compared to conventional texturing [19]. To reduce reflections further, a stack of SiN_x layers with varying refractive indices can give an increase in J_{SC}. Modeling shows that an increase of at least 2% relative in J_{SC} on module level can be expected relative to the SiN_x layer currently used.

6.2. Emitter recombination

Emitter recombination can be reduced by integrating a selective emitter concept in the ECN-MWT processing. A selective emitter consists of a highly doped P emitter under the metal fingers to secure a good contact, while the P dopant level between the fingers is significantly reduced. With good surface passivation, reduction of the dopant level in the emitter results in a significant reduction of J_{0e} and, therefore, significant increase in V_{OC}. An increase in J_{SC} of 1% relative can be expected as compared to the current emitter, but is negligible on module level as all light of wavelengths below 400 nm will be absorbed by the EVA. As described above, only a significant gain on module can be expected if a different encapsulant, like silicone, is used. Based on modeling, the gain in V_{OC} can be expected to be up to 5% relative if the emitter recombination (including the surface) is the only limiting factor for the V_{OC}.

6.3. Rear-side passivation and reflection

The rear side can be improved by replacing the Al-BSF with a passivating layer with a very high reflection. A SiO_x/SiN_x or SiO_x/AlO_x coating improves the rear-side reflection from 77% to 90–95%, improving the J_{SC} with 2.5% relative [32]. Combined with the improved rear-side passivation, a total increase in J_{SC} of 3–4% has already been demonstrated. Due to the improved passivation also the V_{OC} improves slightly around 1–2% relative [33–35].

Combining the different optimization steps can lead to efficiencies of over 20% on cell level and over 19% on module level. For mc-Si, 20.3% cell efficiency was demonstrated by Schultz *et al.* [36] on small area and using special laboratory processes.

7. CONCLUSION

Improvements on all steps in the cell processing resulted in an efficiency increase of more than 2% absolute since 2006. The average efficiency of more than 80 mc-Si ECN-MWT cells, sized 243 cm^2, is 17.6% with a top efficiency of 17.9%.

Using 36 of these cells that had an average efficiency of 17.8% a high-module efficiency was obtained of 17.0%, which was the world record end 2009 and early 2010 in his category. Also various modules were made, also using thinner cells, with 100% yield.

In the future, further improvements can be made in the ECN-MWT process flow by improving the front- and rear-side reflection and reducing the emitter and rear-side recombination. With these improvements cell efficiencies over 20% and module efficiencies over 19% are within reach.

ACKNOWLEDGEMENTS

This work was carried out in the framework of the Crystal Clear Integrated Project and the EOS-ES Starfire project. The EC and the Dutch AgentschapNL are both acknowledged for the financial support under respective contract numbers SES6-CT 2003-502583 and S063024. Royal DSM N.V. was acknowledged for the special anti-reflection coating on the module glass. The REC Group was acknowledged for their material and financial support.

REFERENCES

1. Weeber AW, Kinderman R, de Jong PC, Tool CJJ. 17% Cell efficiencies on large back-contacted multi-crystalline silicon solar cells. *Proceedings of the 21st European Photovoltaic Solar Energy Conference and Exhibition*, Dresden, 2006; 605.
2. Kyocera, Kyoto, Japan, http://www.kyocera.com, Date 30-06-2010.
3. Photovoltech, Tienen, Belgium, http://www.photovoltech.be, Date 30-06-2010.
4. Clement F, Menkoe M, Kubera T, Harmel C, Hoenig R, Wolke W, Wirth H, Biro D, Preu R. Industrially feasible multi-crystalline metal wrap through (MWT) silicon solar cells exceeding 16% efficiency. *Solar Energy Materials and Solar Cells* 2009; **93**: 1051.
5. Bultman JH, Eikelboom DWK, Kinderman R, Tip AC, Tool CJJ, van den Nieuwenhof MACJ, Schoofs C, Schuurmans FM, Weeber AW. Fast and easy single step module assembly for back-contacted c-si solar cells with conductive adhesives. *Proceedings of the 3rd World Conference on Photovoltaic Energy Conversion*, Osaka, 2003; 4O- D13-03.
6. de Jong PC, Eikelboom DWK, Kinderman R, Tip AC, Bultman JH, Meuwissen MHH, van den Nieuwenhof MACJ. Single-step laminated full-size PV modules made with back-contacted mc-Si cells and conductive adhesives. *Proceedings of the 19th European Photovoltaic Solar Energy Conference and Exhibition*, Paris, 2004; 2145.
7. Bennett IJ, de Jong PC, Kloos MJH, Stam CNJ, Gomez RJ, Sanchez-Friera P, Lalaguna B, Schmidt H. Low-stress interconnection of solar cells. *Proceedings of the 22nd European Photovoltaic Solar Energy Conference and Exhibition*, Milan, 2007; 4AV3-V31.
8. Tjengdrawira C, Kloos M, Manshanden P, Erlbaum J. Direct performance comparison of MWT and H-pattern Solar Modules. *Proceedings of the 19th Photovoltaic Science and Engineering Conference and Exhibition*, 2009; 71.
9. Green MA, Emery K, Hishikawa Y, Warta W. Solar cell efficiency tables (version 35). *Progress in Photovoltaics* 2010; **18**: 144.
10. Green MA, Emery K, Hishikawa Y, Warta W. Solar cell efficiency tables (version 36). *Progress in Photovoltaics* 2010; **18**: 346.
11. Schmich E, Gassenbauer Y, Ramspeck K, Dressler K, Fiedler M, Hefner W, Manole M, Bethmann B, Parr E, Schlenker E, Roth P, Schum B, Horzel J, Moschner J, Metz A, Schmidt W. Industrial multi-crystalline silicon solar cells with dielectrically passivated rear side and efficiencies above 18%. *Proceedings of the 25th European Photovoltaic Solar Energy Conference and Exhibition*, Valencia, 2010; 1154.
12. del Cañizo C, del Coso G, Sinke WC. Crystalline Silicon solar module technology: towards the 1 euro per watt-peak goal. *Progress in Photovoltaics* 2009; **17**: 199.
13. Eerenstein W, Bennett IJ, Veldman D, Visser T, Brockholz B, de Jong PC, Copetti CA, Wijnen P. Climate chamber test results of MWT back contact modules. *Proceedings of the 25th European Photovoltaic Solar Energy Conference and Exhibition*, Valencia, 2010; 4CO. 19.5.
14. Späth M, de Jong PC, Bennett IJ, Visser TP, Bakker J, Verschoor AJ. First experiments on module assembly line using back-contact solar cells. *Proceedings of the 23rd European Photovoltaic Solar Energy Conference and Exhibition*, Valencia, 2008; 2917.
15. ASTM Standard E948-09. Standard Test Method for Electrical Performance of Photovoltaic Cells Using Reference Cells Under Simulated Sunlight, ASTM International, West Conshohocken, USA-PA, http://www.astm.org, Date 10-06-2010.
16. Green MA, Emery K, Hishikawa Y, Warta W. Solar cell efficiency tables (version 33). *Progress in Photovoltaics* 2009; **17**: 85.
17. Sinton Instruments, Boulder, USA-CO, http://www.sintoninstruments.com, Date 10-06-2010.
18. Sinton RA. Testing Solar Cell Wafers After Phosphorus Diffusion. April 27, 2004; Application note developed under DOE subcontract ZDO-2-30628-08. http://www.sintoninstruments.com. Unpublished.
19. Tool CJJ, Coletti G, Granek FJ, Koppes M, Kossen EJ, Rieffe HC, Romijn IG, Weeber AW. 17% mc-Si solar cell efficiency using full in-line processing with improved texturing and screen-printed contacts on high-ohmic emitters. *Proceedings of the 20th European Photovoltaic Solar Energy Conference and Exhibition*, Barcelona 2005; 578.
20. Dziewior J, Schmid W. Auger coefficients for highly doped and highly excited silicon. *Applied Physics Letters* 1977; **31**: 346.
21. Green MA. Solar Cells. Prentice-Hall: Englewood Cliffs, 1998; 150–151.

22. Romijn IG, Soppe WJ, Rieffe HC, Burgers AR, Weeber AW. Passivating mc-Si solar cells using SiNx:H: from magic to physics. *Proceedings of the 20th European Photovoltaic Solar Energy Conference and Exhibition*, Barcelona, 2005; 1352.
23. Dekkers HFW, Carnel L, Beaucarne G, Beyer W. Diffusion mechanism of hydrogen through PECVD SiNx:H for a fast defect passivation of mc-Si solar cells. *Proceedings of the 20th European Photovoltaic Solar Energy Conference and Exhibition*, Barcelona, 2005; 721.
24. Hong J, Kessels WMM, Soppe WJ, Weeber AW, Arnoldbik WM, van de Sanden MCM. Influence of the high-temperature ''firing'' step on high-rate plasma deposited silicon nitride films used as bulk passivating antireflection coatings on silicon solar cells. *Journal of Vacuum Science and Technology, B* 2003; **21**: 2123.
25. Lamers MWPE, Romijn IG, Gagliardo M, van den Donker MN, Tool CJJ, Weeber AW. Going to a finite source emitter: improved emitter technology by reduction of the dead P-layer for high-efficiency crystalline silicon solar cells. *Proceedings of the 23rd European Photovoltaic Solar Energy Conference and Exhibition*, Valencia, 2008; 1708.
26. Schubert G, Huster F, Fath P. Silver thick film contact formation on lowly doped phosphorous emitters. *Proceedings of the 20th European Photovoltaic Solar Energy Conference and Exhibition*, Barcelona, 2005; 813.
27. Mewe AA, Romijn IG, Wijnen P, van den Donker MN, van Eijk P, Kerp H, Shaikh A, Weeber AW. MWT ''plug'' metallization: improved performance and process stability of PUM and ASPIRE cells. *Proceedings of the 23rd European Photovoltaic Solar Energy Conference and Exhibition*, Valencia, 2008; 1756.
28. Fang HC, Liu CP, Chung HS, Huang CL. Effects of fine particle content in Al paste on screen printed contact formation and solar cell performance. *Journal of the Electrochemical Society* 2010; **157**: H455.
29. Lamers MWPE, Mewe AA, Bennett IJ, Koppes M, Romijn IG, de Jong PC, Weeber AW. 17+% Back-contacted cells resulting in new world record module efficiency of 16.4%. *Proceedings of the 19th Photovoltaic Science and Engineering Conference and Exhibition*, Jeju, 2009; 32.
30. Grunow P, Krauter S. Modelling of the encapsulation factors for photovoltaic modules. *Proceedings of the IEEE 4th World Conference on Photovoltaic Energy Conversion*, Hawaii, 2006; 2152.
31. McIntosh KR, Cotsell JN, Cumpston JS, Norris AW, Powell NE, Ketola BM. An optical comparison of silicone and EVA encapsulants for conventional silicon PV modules: a ray-tracing study. *Proceedings of the 34th IEEE Photovoltaic Specialists Conference*, Philidephia, 2009; 544.
32. Tool CJJ, Burgers AR, Manshanden P, Weeber AW. Effect of wafer thickness on the performance of mc-Si solar cells. *Proceedings of the 17th European Photovoltaic Solar Energy Conference and Exhibition*, Munich, 2001; 1551.
33. Rentsch J, Schultz O, Grohe A, Biro D, Preu R, Willeke GP. Technology route towards industrial application of rear passivated silicon solar cells. *Proceedings of the IEEE 4th World Conference on Photovoltaic Energy Conversion*, Hawaii, 2006; 1008.
34. Choulat P, Agostinelli G, Ma Y, Duerinckx F, Beaucarne G. Above 17% industrial type PERC Solar Cell on thin multi-crystalline silicon substrate. *Proceedings of the 22nd European Photovoltaic Solar Energy Conference and Exhibition*, Milan, 2007; 1011.
35. Romijn IG, Lamers MWPE, Stassen A, Mewe AA, Koppes M, Kossen E, Weeber AW. ASPIRe: a new industrial MWT cell technology enabling high efficiencies on thin and large mc-Si wafers. *Proceedings of the 22nd European Photovoltaic Solar Energy Conference and Exhibition*, Milan, 2007; 1043.
36. Schultz O, Glunz SW, Willeke GP. Multicrystalline silicon solar cells exceeding 20% efficiency. *Progress in Photovoltaics* 2004; **12**: 553.